

## NUMERICAL SIMULATION OF GAS FLOW IN AN ELECTROSTATIC PRECIPITATOR

Q. F. HOU<sup>1\*</sup>, B.Y. GUO<sup>1</sup>, L.F. LI<sup>2</sup> and A. B. YU<sup>1</sup>

<sup>1</sup>Laboratory for Simulation and Modelling of Particulate Systems, School of Materials Science and Engineering,  
The University of New South Wales, Sydney, NSW 2052, Australia

<sup>2</sup>Longking Co. Ltd, Longyan, Fujian, China

\*Corresponding author, E-mail address: Q.Hou@student.unsw.edu.au

### ABSTRACT

Electrostatic precipitator (ESP) system is widely used in power generation and metallurgical industries to reduce dust emission in the flue gas. The main body of an ESP unit typically consists of a large chamber and a number of internal parts: perforated plates, electrodes and channel plates. Uniform distribution of gas flow is expected in the design of the ESP unit to achieve its best collecting performance. Traditional step-by-step scale-up of experimental rig is costly and time-consuming. This paper presents a multi-scale approach to numerically simulate the gas flow in an ESP system with two parallel ESP units. Firstly, the flow resistance coefficients of the perforated plates with different porosities and of the channel plate are obtained through unit cell studies. The results are validated against an empirical equation. Secondly, the simplification of the perforated plates as porous jump boundaries is justified using a simple ESP experimental rig and it is found that the anisotropic porous media boundary has similar behaviour while it is more convenient to control porosity distribution of the perforated plates. Finally, another pilot scale test rig with all internal parts is built to measure the flowrates in each branch. The numerical approach is validated by comparing the measured and predicted flowrates in each branch.

*Keywords:* Electrostatic precipitator; Numerical modelling; Multi-scale approach; Perforated plates.

### INTRODUCTION

Electrostatic precipitator (ESP) device is widely used in industries, such as metallurgy and power generation, to reduce dust emission in the flue gas. Its performance greatly depends on the design of the complex structures: such as the perforated plates in the diffuser, electrodes in the collecting chamber, hoppers, the channel plates in the contraction section, and piping system. The perforated plates and piping system are designed in a way to guarantee uniform flow distribution between different ESP units and uniform flow field in the collecting chambers. Due to the complicated geometry in the ESP unit, a single experimental model is hard to consider all the parts. In the past, some experimental works were carried out to investigate the design of ESP focusing on only a few parts and parameters, for example the pressure drop through

perforated plates and flow field in the diffuser (Rao and Rao, 1972; Sahin, 1989; Sahin and Ward-Smith, 1993; Seltam, 1995), the effects of the hole shape of the perforated plate on pressure drop (Gan and Riffat, 1997) and the velocity distribution in a diffuser (Noui-Mehidi et al., 2005). The designing method of a complete device, usually by trial and error experiments, is very expensive and time-consuming. Alternatively, computational fluid dynamics (CFD) provides a cheaper way to tackle these problems. Recently, CFD method has been used to provide more detailed information and to save the expense and time span for the development of an ESP system (Park and Kim, 2000; Varonos et al., 2002; Nikas et al., 2005; Skodras et al., 2006; Haque et al., 2009). However, most of these studies either used two dimensional numerical models or simplified perforated plates as porous jump boundaries. In the latter case, the empirical coefficients have to be applied. Furthermore, such one-dimensional simplification of porous media (PM) only considers the resistance in the normal direction to porous face (ANSYS, 2009). Hence, its application to perforated plates needs to be justified for the complicated geometry and flow around them.

In the present work, a computational strategy is proposed and validated for gas flow in the ESP system, in order to obtain more reliable results with a minimum computational effort. A multi-scale approach comprising three stages is developed within ANSYS FLUENT environment (ANSYS, 2009). The model starts with unit cell studies to build up the correlations of pressure drop and velocity for the perforated plates and channel plates used in an ESP unit. Then, with these correlations implemented as porous jump boundary, a single ESP unit is simulated and a correlation describing the pressure drop of the single unit and flow rate is established. Finally, a larger-scale model considers two parallel ESP units as PM and the piping system, and subsequently the distribution of flowrates between the two units is obtained.

### ESP SYSTEM DESCRIPTION

The dimensions of the model geometry are obtained according to an experimental test rig in Longking Co. Ltd of China. The key structures of the ESP unit are considered and the generated surface meshes are illustrated in Figure 1. There are inlet, outlet, hoppers, perforated plates, channel plates and electrodes. A piping system is connected both upstream and downstream. The geometry is very complicated and it is difficult to

implement all the details exactly in a single CFD model, particularly the perforated plates and channel plates with thousands of holes/cells. The unit cell study aims to simplify the boundary condition and minimize the

computational effort. For all the cases in this paper, the turbulent flow is assumed and two-equation model is adopted, such as  $k-\omega$  model.

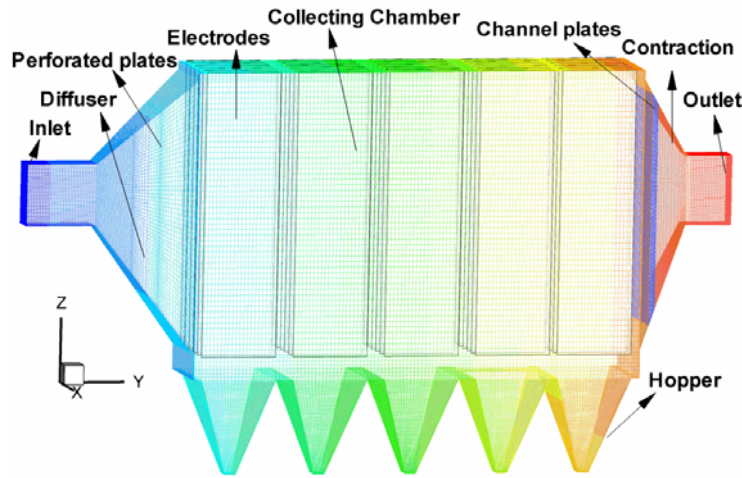


Figure 1: ESP unit and mesh.

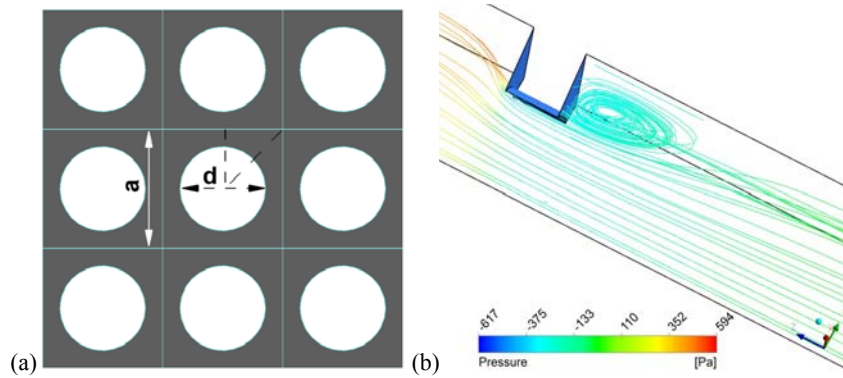


Figure 2: Selection of the unit cell from the perforated plate: (a) dimensions (b) streamlines.

### PERFORATED PLATES MODELLING

To determine the parameters of the perforated plates with different open areas (porosities), which are usually measured through physical experiments, mathematical modelling and numerical experiments of a unit cell are carried out. Note, for the perforated plate, the unit cell could be a representative flow domain around a single hole, due to the periodic pattern of the holes. Or even more simply, consideration of one-eighth sector of the hole is sufficient when the unit cell is fully symmetric. Figure 2 shows the dimensions of the selected unit cell and predicted streamlines. The porosity of the perforated plate is determined by  $\pi d^2/4a^2$ . The streamlines show a circulation zone after the contraction, which may cause an additional pressure drop. The pressure drop through the unit cell is evaluated as the pressure difference between the inlet and outlet. Since the wall friction in a channel flow is relatively small, the pressure drop thus obtained is considered as the pressure drop through the perforated plates. Various inlet velocities and porosity (30%, 40% and 50%) are tested to determine the parameters in the pressure drop equation (or quadratic equation),  $\Delta P = (\mu/\alpha v + 1/2 C_2 \rho v^2) \cdot \Delta m$  for setting the coefficients. The more details of this equation can be found in the FLUENT's

user guide (ANSYS, 2009). Figure 3 shows that the pressure drop increases with an increase in inlet gas velocity and a decrease in porosity. The corresponding parameters, determined by curve-fitting using the above relation, are given in Table 1 for the stream-wise direction.

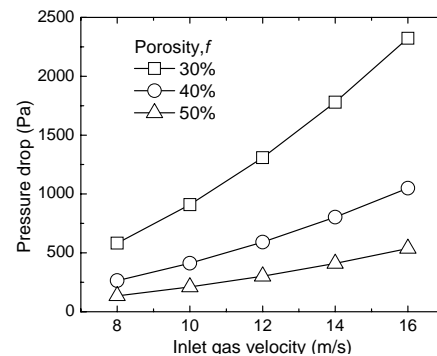


Figure 3: Relations between inlet gas velocity and pressure drop under different porosities.

According to an empirical correlation for resistant coefficient  $\xi = 1/(f \times c)^2 - 1$  and pressure drop  $\Delta P = \xi \times 1/2 \rho v^2$ ,

where the  $f$  is the porosity and  $c$  is the contraction coefficient (Idelchik, 1994), the empirical and numerical coefficients of the resistance are compared for three different porosities of the plates.  $c = 0.85$  is adopted for circular holes. As shown in Figure 4, the variations of resistance coefficient with porosity have a similar trend.

Porosity, %	30	40	50
$C_2, m^{-1}$	$1.00 \times 10^4$	$4.51 \times 10^3$	$2.31 \times 10^3$
$\alpha, m^2$	$5.60 \times 10^{-7}$	$7.56 \times 10^{-7}$	$9.40 \times 10^{-6}$

**Table 1:** The coefficients in the pressure drop equation under different porosities in the stream-wise direction.

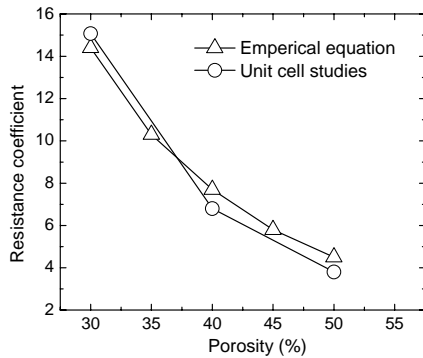


**Figure 4:** Comparison of resistance coefficients by empirical equation and unit cell studies of perforated plates.

The perforated plates were usually simplified as porous jump boundaries in ESP unit studies (e.g. Haque et al., 2009), which calculate the resistance based on the velocity normal to the porous surface (ANSYS, 2009). Although they gave reasonable results, it is difficult to implement, in the current version of FLUENT software, the variation in porosity over a perforated plate by porous jump boundary, which is often practised to control the flow field in some ESP applications. Instead, it can be easily realized in an anisotropic porous media zone model by user defined function. The flow resistance in the porous media is consistent with the porous jump model. The predictions are compared between the two approaches.

A simplified ESP test rig is built without the electrodes, hoppers and channel plates. In this model, each perforated plate has its uniform porosity distribution; from inlet to outlet, the porosities of the perforated plates are 50%, 40% and 30% respectively. The geometry of the test rig, the planes and grid for the measurement of velocities are shown in Figure 5. The flow field behind the diffuser is measured based on a  $12 \times 15$  test grid on the planes with an uniform inlet velocity at 30 m/s and the measured results are given in Figure 6a. The measured results show non-uniform distributions with smaller velocity at the central region. Figure 6b shows the results for the case with porous jump boundaries for the perforated plates. The results show consistent distribution with measured ones. Figure 6c shows the result by a so called “anisotropic porous media” model without considering the transverse resistance. It is shown that both the porous jump model and the porous media model are consistent and agree well

with the measured results. The application of the porous media model to simulate the perforated plates is justified as reasonable. This allows the simulation of the perforated plate with porosity distribution by user defined function.

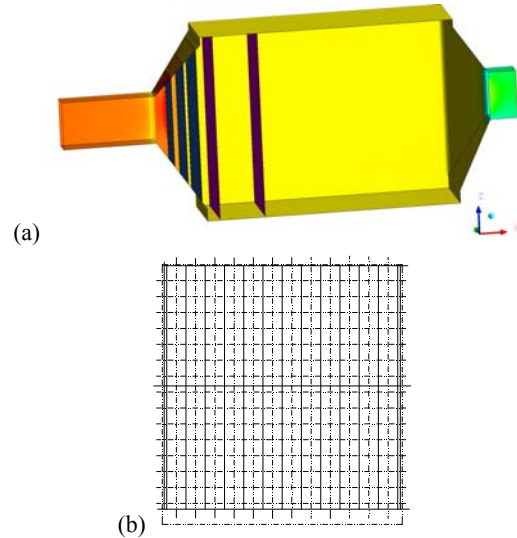


**Figure 5:** Geometry of the simplified ESP test rig and the positions of measurement planes (a) and the grid (b).

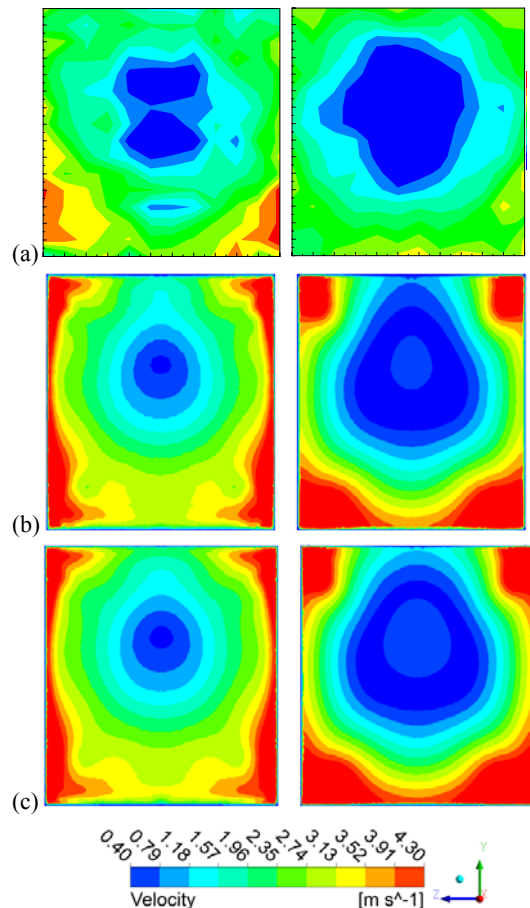


**Figure 6:** Measured and predicted velocity fields in the simple ESP model: (a) measured; (b) predicted by porous jump model; (c) predicted by the anisotropic porous media model.

## CHANNEL PLATES MODELLING

The channel plate at the entry of the downstream contracting section consists of an array of channel shaped materials. The resistance force can also be determined by unit cell modelling. The resistance can be considered respectively in three directions (Figure 7), namely, stream-wise (y), transverse (x) and channel-wise (z).

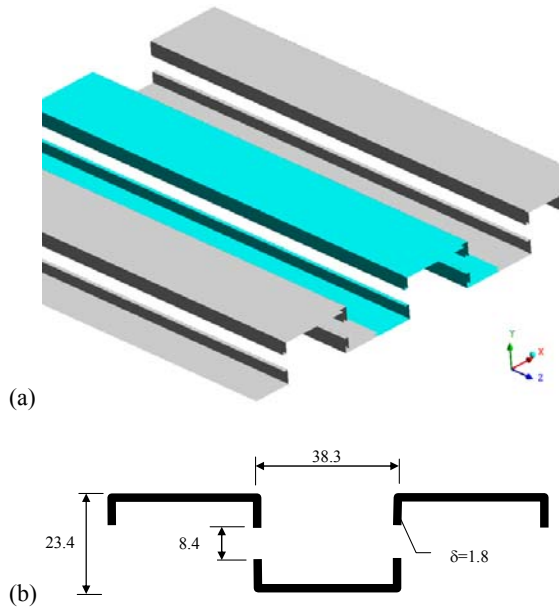


**Figure 7:** A surface visualization of channel plates (a) and dimensions of a unit (b).

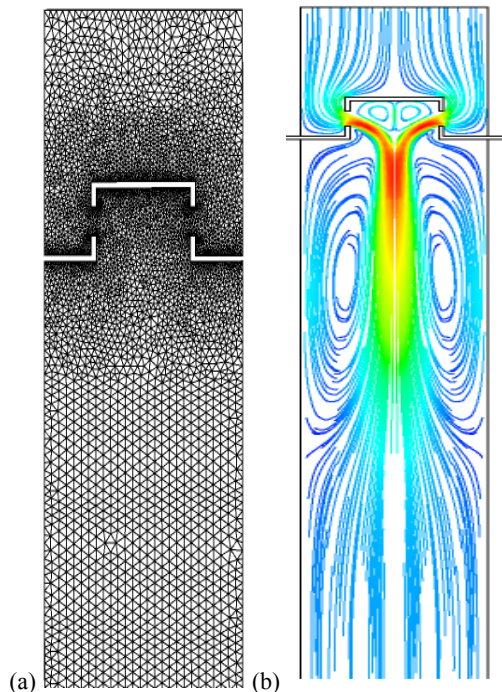


**Figure 8:** Mesh and results for unit cell study of channel plate: (a) mesh; (b) streamlines.

Generally, many recirculating eddies exist downstream behind the channels. Figure 8 shows the generated mesh and a typical streamline result for channel plate simulation

in stream-wise direction. With the mean velocity in the range from 0.50 to 1.50 m/s, the curve-fitting for the case of symmetric flow gives the value of  $\alpha$  as  $1.21 \times 10^{-6} \text{ m}^2$  and the value of  $C_2$  as  $2152.76 \text{ m}^{-1}$  in the stream-wise direction.

In the transverse direction, a typical flow pattern is shown in Figure 9. The force per square meter of volume occupied by the channels can be roughly expressed by a fitted correlation  $S = 2.59v^2$ , where  $v$  is the velocity component in the transverse direction. Then, the determined value of  $1/\alpha$  is  $0 \text{ m}^2$  and the value of  $C_2$  is  $4.29 \text{ m}^{-1}$  in the transverse direction.

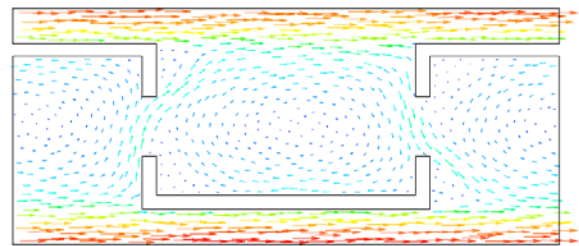


**Figure 9:** Typical transverse flow pattern.

In the channel-wise direction, the pressure drop resistance can be estimated through the boundary layer theory. In the present simulation conditions, turbulent boundary layer is assumed. The drag coefficient  $C_D$  is given by  $0.072(\text{Re})^{-1/5}$  from Prantl's one-seventh-power law (Schlichting, 1979). Then, the quadratic curve fitting gives the value of  $1/\alpha$  as  $291.58 \text{ m}^2$  and the value of  $C_2$  as  $4.12 \times 10^{-3} \text{ m}^{-1}$  according to the form of pressure drop equation. The average wall surface area per channel plate volume is calculated as  $118.94 \text{ m}^2/\text{m}^3$ .

## ESP UNIT MODELLING

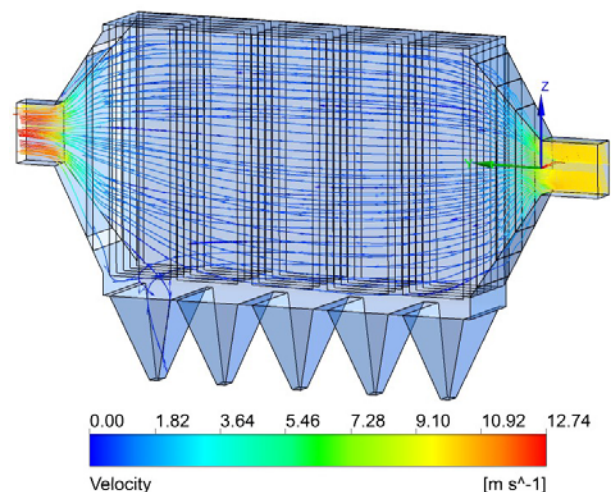


**Figure 10:** Streamline colored by the magnitude of velocity, where the inlet velocity is 10 m/s.

In the present work, only one half of an ESP unit is considered based on symmetry boundary conditions. The origin of the coordinate is in the centre of the inlet surface. The parameters determined in the unit cell studies can be

implemented into three porous media boundaries for the perforated plates according to their porosity and distributions (ANSYS, 2009). The channel plate is implemented as a single PM region. To minimize the effects of inlet velocity profile, the inlet channel has been extended by 0.3 m. Figure 10 shows the streamlines in an ESP model at an inlet velocity of 10 m/s. The flow appears to be quite uniform in the collecting chamber. Note that in the present model, the baffles in the hoppers are not considered and this may cause the re-trap of dust. More detailed structures will be considered in the future work.

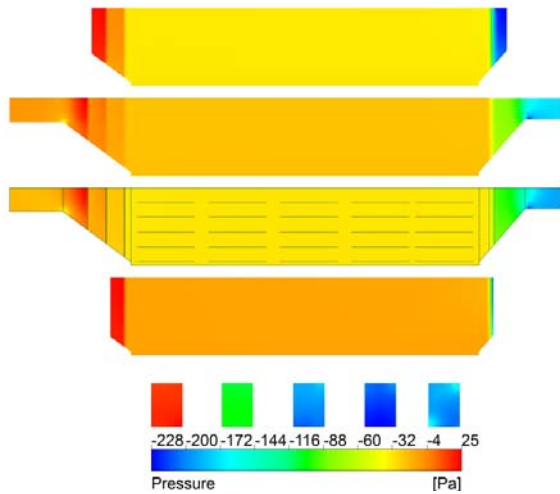


**Figure 11:** Pressure distributions of sliced xy planes, where z are 0.3, 0.1, 0.0, -0.5 and -1.0 m from top to bottom, respectively.

The overall pressure drop through the ESP unit is an important index in its application. Figure 11 shows that the pressure drop is mainly caused by the perforated and channel plates. On the other side, the uniform distribution of pressure field is also important. Figure 11 also shows that the pressure drop distribution from top to bottom in the ESP unit is very complicated. The average pressure between the hoppers differs greatly among different hoppers. (Refer to the bottom-most row one in Figure 11).

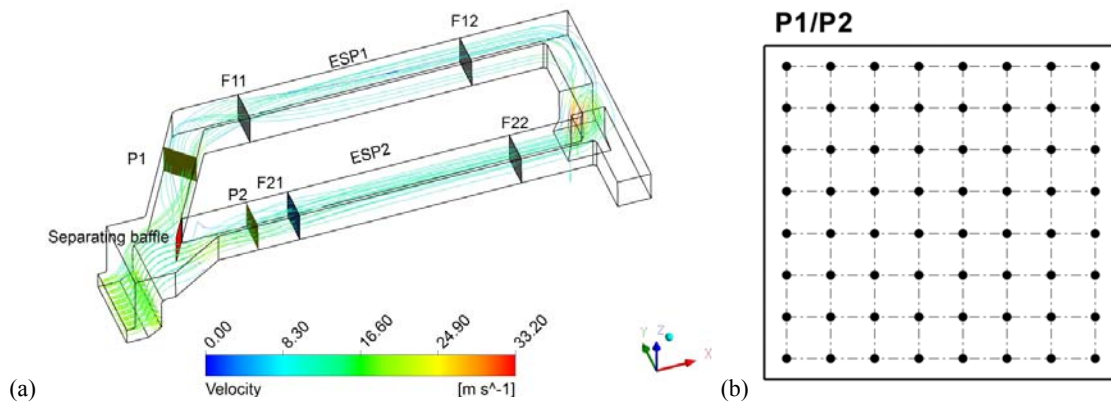


**Figure 13:** Configuration of the whole system and the streamline colored by the magnitude of velocity (a) and the test grid (b), where the inlet velocity is 20 m/s.

To minimize the computational load, the ESP unit is considered as a uniform PM zone. A series of simulations are carried out and the predicted relation of the pressure drop and velocity is given in Figure 12. Then, the value for  $C_2$  is obtained as  $0.69 \text{ m}^{-1}$  and the value for  $1/a$  is  $1.43 \times 10^4 \text{ m}^{-2}$  in the stream-wise direction.

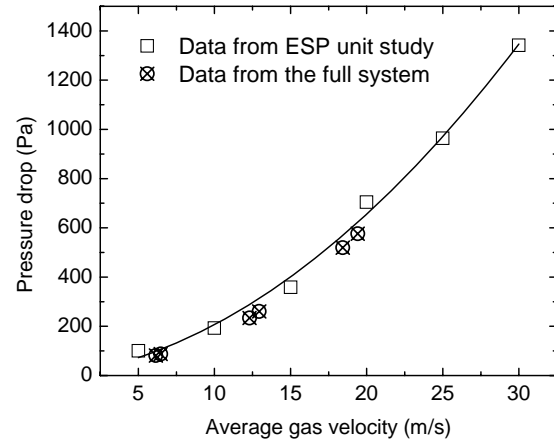


**Figure 12:** The relation of pressure drop of an ESP unit with the average velocity.

## SYSTEM MODELLING

An equal flow rate between the two parallel ESP units is desirable to maintain an even load to each ESP unit. A larger scale model including the piping system is considered to calculate the flow rate distribution. The two ESP units are treated as PM boundaries. Faces F11 and F12 in Figure 13 denote the positions of the inlet and outlet planes of the ESP unit 1 and Faces F21 and F22 are for unit 2, where the pressures and velocities are obtained. A separating baffle is installed to adjust the distribution of flow rate between the two branches. Figure 13 shows that the streamlines distribute quite uniformly in the two ESP units. Under the present condition, the mass flow rates are 1.78 kg/s in ESP1 and 1.86 kg/s in ESP2 respectively, at an inlet velocity of 20 m/s. The deviation between two branches, defined by  $(Q_1 - Q_2)/(Q_1 + Q_2) \times 100\%$ , is within 3%.

## VALIDATION AND DISCUSSION

The reliability of treating the ESP units as uniform PMs is investigated by running three different cases with the inlet velocities of 10, 20 and 30 m/s respectively. The pressure drops through the PMs are obtained for each branch and given in Figure 12. The results show that the pressure drops obtained are distributed near the fitting curve. This indicates that the uniform PM represents the ESP unit in terms of pressure drop is reasonable.

To validate the present multi-scale approach, the pressures on two planes before the entry to ESP unit are measured using a Pitot pressure gauge. In the test rig, the inlet velocity is 20 m/s. The experimental data is retrieved at positions based on an 8×8 Grid on the planes P1 and P2 (Figure 13). The dynamic pressure can be used to calculate the flowrates in different ESP branches. When the ESP units are treated as uniform PMs, the predicted distributions of pressure at P1 and P2 may not match exactly the measured one at each measuring point. The effects of the inlet profile and geometry on the pressure distributions will be considered in the future work. The main purpose of the full system modelling is to investigate the flow rate distribution between the two branches at the present stage. The predicted and measured flowrates (Q) are compared in Table 2. Their deviations are within 5%. It also shows that the use of a separating baffle makes the flow distribution quite uniform.

	Measured Q (kg/s)	Predicted Q (kg/s)
P1	1.86	1.78
P2	1.96	1.86

**Table 2:** Comparisons of the flowrates in two branches measured from planes P1 and P2.

## CONCLUSION

A multi-scale mathematical modelling approach is applied to the simulation of gas flow in an ESP system. The work is divided into three steps, i.e. unit cell studies of perforated plates and the channel plate, ESP unit modelling, and the whole system including multiple ESP units and the piping system. The consistency of the pressure drop through the PMs in the full system and the fitting curve in ESP unit study justifies the simplification of the ESP unit as a uniform porous media. The proposed multi-scale approach is validated by experimental data and empirical correlation.

## ACKNOWLEDGEMENTS

The financial support from Longking Co. Ltd is gratefully appreciated, and Q. F. Hou is grateful to the University of New South Wales for providing University Postgraduate Awards.

## REFERENCES

- ANSYS, 2009. ANSYS Fluent 12.0 User's Guide.  
GAN, G.H. and RIFFAT, S.B., (1997), "Pressure loss characteristics of orifice and perforated plates". *Exp. Therm. Fluid Sci.*, 14, 160-165.  
HAQUE, S.M.E., RASUL, M.G., KHAN, M.M.K., DEEV, A.V. and SUBASCHANDAR, N., (2009),

"Influence of the inlet velocity profiles on the prediction of velocity distribution inside an electrostatic precipitator". *Exp. Therm. Fluid Sci.*, 33, 322-328.

IDELCHIK, I.E., 1994. Handbook of hydraulic resistance. CRC Press Inc., New York.

NIKAS, K.S.P., VARONOS, A.A. and BERGELES, G.C., (2005), "Numerical simulation of the flow and the collection mechanisms inside a laboratory scale electrostatic precipitator". *J. Electrostatics*, 63, 423-443.

NOUI-MEHIDI, M.N., WU, J., SUTALO, I.D. and GRAINGER, C., (2005), "Velocity distribution downstream of an asymmetric wide-angle diffuser". *Exp. Therm. Fluid Sci.*, 29, 649-657.

PARK, S.J. and KIM, S.S., (2000), "Electrohydrodynamic flow and particle transport mechanism in electrostatic precipitators with cavity walls". *Aerosol Sci. Technol.*, 33, 205-221.

RAO, C.D. and RAO, C.V., (1972), "Pressure-drop studies on a single perforated plate". *Indian J. Technol.*, 10, 1-&.

SAHIN, B., (1989), "Pressure losses in an isolated perforated plate and jets emerging from the perforated plate". *Int. J. Mech. Sci.*, 31, 51-61.

SAHIN, B. and WARD-SMITH, A.J., (1993), "The pressure distribution in and flow characteristics of wide-angle diffusers using perforated plates for flow control with application to electrostatic precipitators". *Int. J. Mech. Sci.*, 35, 117-127.

SCHLICHTING, H., 1979. Boundary Layer Theory. McGraw-Hill, New York.

SELTSAM, M.M., (1995), "Experimental and theoretical study of wide-angle diffuser flow with screens". *AIAA J.*, 33, 2092-2100.

SKODRAS, G., KALDIS, S.P., SOFIALIDIS, D., FALTSI, O., GRAMMELIS, P. and SAKELLAROPOULOS, G.P., (2006), "Particulate removal via electrostatic precipitators - CFD simulation". *Fuel Process. Technol.*, 87, 623-631.

VARONOS, A.A., ANAGNOSTOPOULOS, J.S. and BERGELES, G.C., (2002), "Prediction of the cleaning efficiency of an electrostatic precipitator". *J. Electrostatics*, 55, 111-133.